Formation of the First Galaxies: Metal Enrichment and Stellar Populations

John H. Wise[*]
Department of Astrophysical Sciences, Princeton University, Princeton, NJ 08544, USA
E-mail: `jwise@astro.princeton.edu`

Matthew J. Turk and Michael L. Norman
Center for Astrophysics and Space Sciences, University of California at San Diego, La Jolla, CA 92093, USA
E-mail: `matthewturk@gmail.com`

Tom Abel
Kavli Institute for Particle Astrophysics and Cosmology, Stanford University, Menlo Park, CA 94025, USA
E-mail: `tabel@stanford.edu`

We present adaptive mesh refinement radiation hydrodynamics simulations that follows the transition from Population III to II star formation. We model stellar radiative feedback with adaptive ray tracing. A top-heavy initial mass function for the Population III stars is considered, resulting in a plausible distribution of pair-instability supernovae and associated metal enrichment. We find that the gas fraction recovers from 5 percent to nearly the cosmic fraction in halos with merger histories rich in halos above $10^7 M_\odot$. A single pair-instability supernova is sufficient to enrich the host halo to a metallicity floor of $10^{-3} Z_\odot$ and to transition to Population II star formation. This provides a natural explanation for the observed floor on damped Lyman alpha (DLA) systems metallicities reported in the literature, which is of this order. We find that stellar metallicities do not necessarily trace stellar ages, as mergers of halos with established stellar populations can create superpositions of $t - Z$ evolutionary tracks. A bimodal metallicity distribution is created after a starburst occurs when the halo can cool efficiently through atomic line cooling.

---

[*]Speaker.

---

1. Motivation

The first (Pop III) stars are metal-free and have a large characteristic mass and suppressed fragmentation in its protostellar collapse (Abel et al., 2002; Bromm et al., 2002; O'Shea & Norman, 2007). A fraction of these stars enrich the surrounding intergalactic medium (IGM) when they go supernova, which can happen in stars $\lesssim 40\ M_\odot$ in Type II supernovae (SNe) or in stars roughly between $140\ M_\odot$ and $260\ M_\odot$ in pair-instability SNe (PISNe; Heger & Woosley, 2002a). The host halo and the neighboring halos are then enriched with this ejecta. There exists a critical metallicity that is $\sim 10^{-6} Z_\odot$ if dust cooling is efficient (Omukai et al., 2005; Schneider et al., 2006; Clark et al., 2008) and $\sim 10^{-3.5} Z_\odot$ otherwise (Bromm et al., 2001; Smith et al., 2009), where the gas can cool rapidly, lowering its Jeans mass. An intermediate characteristic mass of $\sim 10\ M_\odot$ can be occur if the gas cooling is suppressed to the cosmic microwave background (CMB) temperature (Larson, 1998; Tumlinson, 2007; Smith et al., 2009). The resulting Population II star cluster will thus have a lower characteristic stellar mass than its metal-free progenitors. These first stellar clusters may be connected to stars in the Milky Way halo and nearby dwarf spheroidal (dSph) galaxies, both with a metallicity floor of [Z/H] = –4 (Beers & Christlieb, 2005; Tafelmeyer et al., 2010; Frebel et al., 2010).

The transition from Pop III to Pop II star formation (SF) is solely dependent on the propagation of metals from the SNe remnants into future sites of SF. Their flows are complex because of the interactions between the SN blastwave, cosmological accretion and halo mergers, and nearby stellar feedback. In minihalos ($M \sim 10^6\ M_\odot$), radiation from a massive Pop III star can drive a 30 km s^{-1} shock, which is 10 times greater than the escape velocity of the halo, and leaves behind a warm (3×10^4 K) and diffuse (0.5 cm^{-3}) medium (Kitayama et al., 2004; Whalen et al., 2004; Abel et al., 2007). This aids in the expansion of the blastwave because it delays the transition to the Sedov-Taylor and snowplow phases. In PISNe, approximately half of the metals stay in the IGM with a metal bubble size of a few kpc (Wise & Abel, 2008; Greif et al., 2010). The blastwave may induce SF in nearby halos through the compression of the gas (Ferrara, 1998), and timescales for metal mixing into the dense gas are many dynamical times (Cen & Riquelme, 2008) for shock velocities $\lesssim 100$ km s^{-1}.

Numerical simulations are useful to detangle and study these complexities and the transition from Pop III to II stars. Here, we present a simulation that includes both types of SF, and their radiative and mechanical feedback. The methods used here incorporate and link together recent results from metal-enriched and metal-free star formation, the critical metallicity, and pair-instability supernovae. This is the first time it has been possible to link the formation and feedback of the first stars to protogalaxies, resolving the important scales and including the most important physical effects.

2. Method

2.1 Simulation setup

We use the adaptive mesh refinement (AMR) code enzo v2.0[1] (O'Shea et al., 2004), which has been modified to use a HLLC Riemann solver (Toro et al., 1994) for additional stability in

---

[1] enzo.googlecode.com, changeset b86d8ba026d6

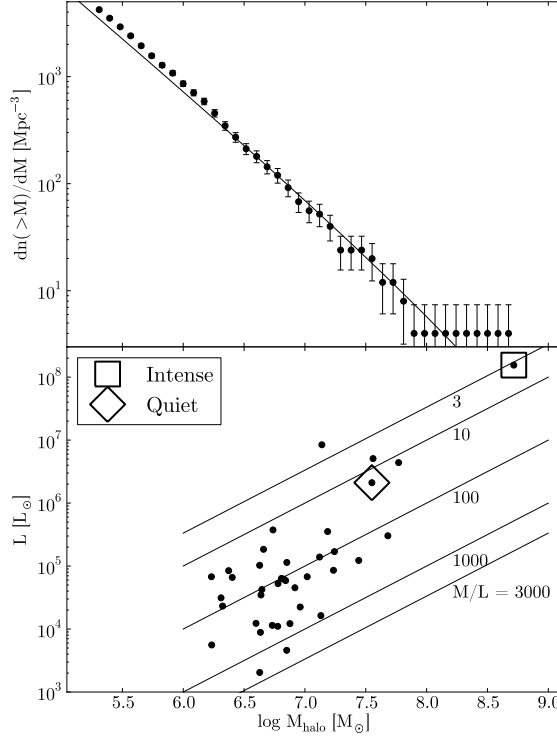<div style="text-align: right">PoS(CRF 2010)030</div>

Figure 1: *Top*: Halo mass function of the simulation compared with the analytical fit (solid) of Warren et al. (2006). *Bottom*: Total Pop II luminosities of halos with constant mass-to-light ratios overplotted.

strong shocks. To resolve minihalos with at least 100 dark matter (DM) particles and follow the formation of the first generation of dwarf galaxies, we use a simulation box of 1 Mpc that has a resolution of 256^3. This gives us a DM mass resolution of $1840\ M_\odot$. We refine the grid on baryon overdensities of $3 \times 2^{-0.2l}$, where l is the AMR level, resulting in a super-Lagrangian behavior. We also refine on a DM overdensity of 3×2^l and always resolve the local Jeans length by at least 4 cells, avoiding artificial fragmentation during gaseous collapses (Truelove et al., 1997). This simulation has 1.4×10^8 computational elements and a maximal spatial resolution of 0.1 pc. We initialize the simulation with *grafic* (Bertschinger, 2001) at $z = 130$ and use the cosmological parameters from the 7-year WMAP data (Komatsu et al., 2010): $\Omega_M = 0.266$, $\Omega_\Lambda = 0.734$, $\Omega_b = 0.0449$, $h = 0.71$, $\sigma_8 = 0.81$, and $n = 0.963$ with the variables having their usual definitions. We stop the simulation at $z = 7$.

We use a non-equilibrium chemistry solver with 9 species of hydrogen, helium, and molecular hydrogen (Abel et al., 1997). We spatially distinguish metal enrichment from Pop II and Pop III stars. We will follow-up this study with one that considers radiative cooling from metal-enriched gas, using the method of Smith et al. (2008).

2.2 Star formation

We distinguish Pop II and Pop III SF by the total metallicity of the densest cell in the molecular cloud. Pop II stars are formed if [Z/H] > -4, and Pop III stars are formed otherwise. We do not consider Pop III.2 stars and intermediate mass stars from CMB-limited cooling.

Simulations have shown that the characteristic mass of Pop III stars $M_{\mathrm{char}} \sim 100\ M_\odot$. They form in molecular clouds that coexist with the dark matter halo center with limited fragmentation occurring during their collapse; however Turk et al. (2009) and Stacy et al. (2010) have recently shown that Pop III binaries may form in a fraction of such halos.

For Pop III stars, we use the same SF model as Wise & Abel (2008) where each star particle represents a single star, forming at an overdensity of 5×10^5. Instead of using a fixed stellar mass, we randomly sampled from an IMF with a functional form of

$$f(M)dM = M^{-1.3} \exp\left[-\left(\frac{M_{\mathrm{char}}}{M}\right)^{1.6}\right] dM \qquad (2.1)$$

to determine the stellar mass. Above M_{char}, it behaves as a Salpeter IMF but is exponentially cutoff below that mass (Chabrier, 2003; Clark et al., 2009). For reproducibility, we record the number of times the random number generator (Mersenne twister; Matsumoto & Nishimura (1998)) has been called for use when restarting the simulations.

We treat Pop II SF with the same prescription as Wise & Cen (2009), which is a modified version of the Cen & Ostriker (1992) method but accounts for the fact that the molecular clouds are resolved. The critical overdensity is the same as the Pop III SF model. In each star-forming region, seven percent of the cold gas ($T < 10^3$ K) is removed from the grid and deposited into the star particle that lives for 20 Myr, the maximum lifetime of an OB star. These stars generate the majority of the ionizing radiation and SNe feedback in stellar clusters, thus we ignore lower mass stars.

2.3 Stellar feedback

We use mass-dependent luminosities and lifetimes of the Pop III stars from Schaerer (2002). The radiation field is evolved with adaptive ray tracing (Abel & Wandelt, 2002; Wise & Abel, 2010) and is coupled self-consistently to the hydrodynamics. We model the H_2 dissociating radiation with an optically-thin, inverse square profile, centered on all stars. These stars die as pair-instability SNe (PISNe) if they are in the mass range 140–260 $M_\odot$ (Heger et al., 2003). We use the explosion energy from Heger & Woosley (2002b), where we fit the following function to their models, $E_{\mathrm{PISN}} = 10^{51} \times [5.0 + 1.304(M_{\mathrm{He}} - 64)]$, where $M_{\mathrm{He}} = (13/24) \times (M_\star - 20)M_\odot$ is the helium core (and equivalently the ejecta) mass and $M_\star$ is the stellar mass.

The Pop II stars emit 6000 hydrogen ionizing photons per baryon over their lifetime, and we do not consider singly- and doubly-ionizing helium photons. We note that low-metallicity stars generate up to a factor of four more ionizing photons than a solar metallicity population (Schaerer, 2003) and might be underestimating the radiative feedback. Nonetheless this study provides an excellent first insight in the transition to Pop II SF, as the metal enrichment is the key ingredient here. For SN feedback, these stars generate 6.8×10^{48} erg s^{-1} $M_\odot^{-1}$ after living for 4 Myr, which is injected into spheres with a radius of 10 pc. If the resolution of the grid is less than 10/3 pc, we deposit the energy into a 3^3 cube surrounding the star particle.
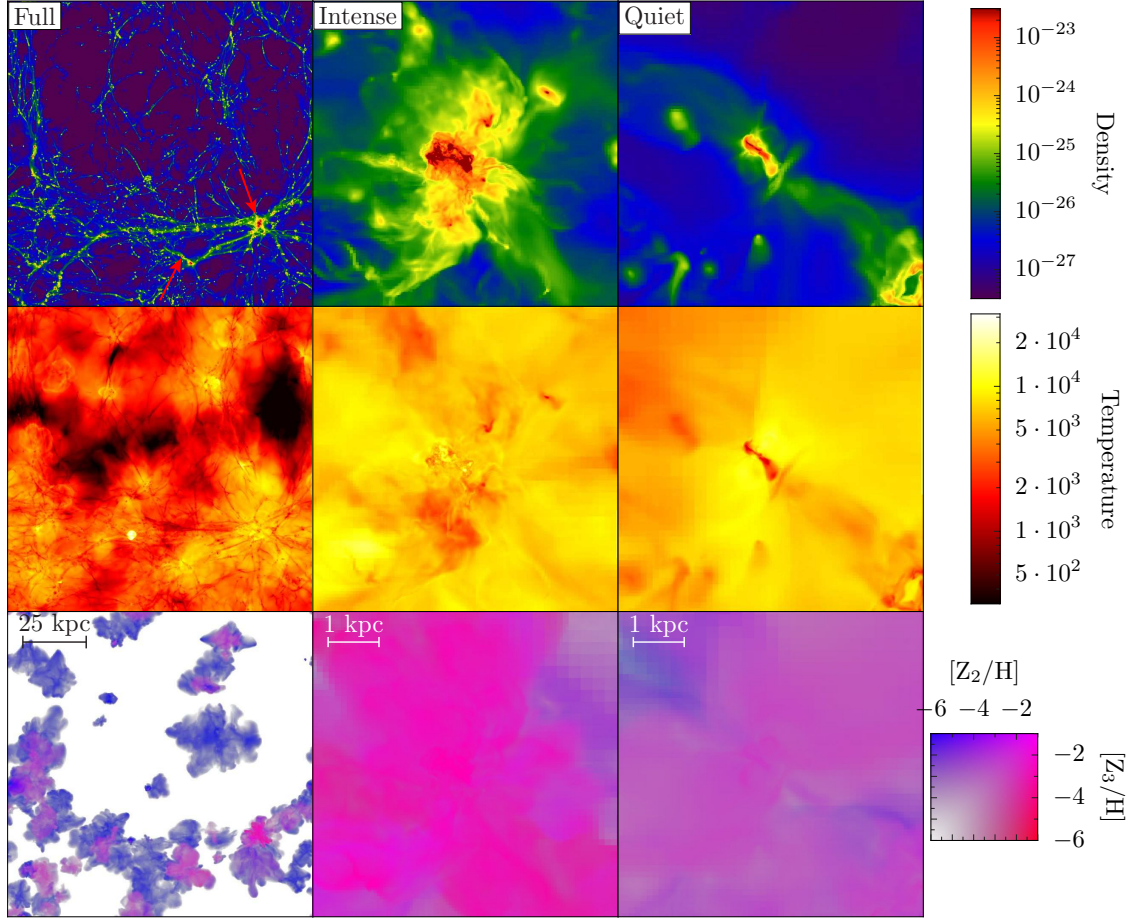
Figure 2: Density-weighted projections of gas density (top), temperature (middle), and metallicity (bottom) at $z = 7$. The left column shows the entire simulation volume, where the center and right columns focus on the intense and quiet halos, which are marked by left and right arrows in the upper-left panel. The metallicity projections are a composite picture of metals originating from Pop III (red) and Pop II (blue) stars with magenta indicating a mixture of the two.

3. Results

Here we present the gaseous and stellar evolution of two selected halos in the simulation: one that has an early mass buildup but no major mergers after $z = 12$, and one that experiences a series of major mergers between $z = 10$ and $z = 7$. We name the halos "quiet" and "intense", respectively. The entire simulation contains 38 galaxies with 3640 Pop II stellar clusters and captures the formation of 333 Pop III stars. The halo mass function and galaxy luminosities are plotted in Figure 1.

We illustrate the state of the simulation at $z = 7$ in Figure 2 with density weighted projections of gas density, temperature, and metallicity, showing the entire box and focusing on the two halos of interest. Radiative and mechanical feedback create a multi-phase medium inside these halos, which are embedded in a warm and ionized IGM.
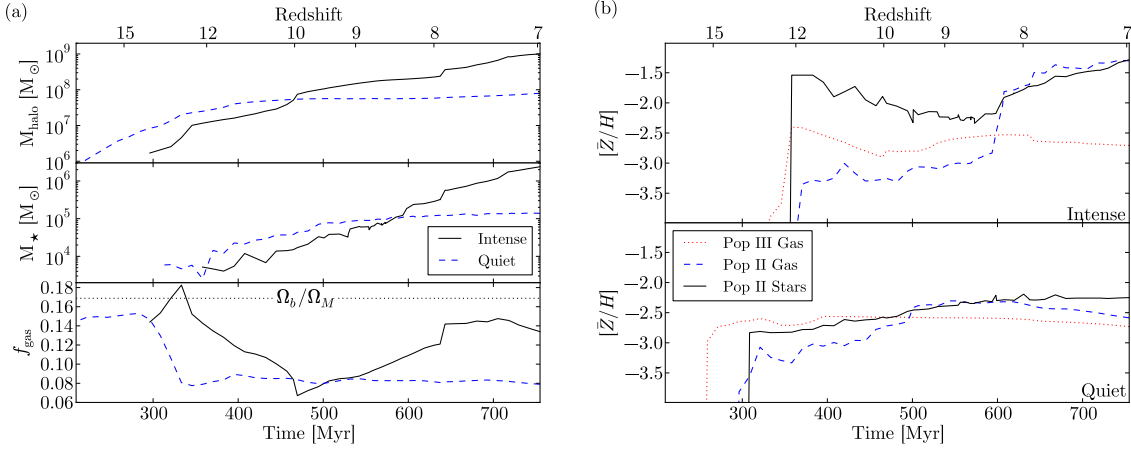
Figure 3: (a) Evolution of the total halo mass (top), stellar mass (middle), and gas fraction (bottom) of the quiet (dashed) and intense (solid) halos. (b) Mass-weighted stellar metallicities and gas metallicities enriched by Pop II and Pop III SNe of the intense (top) and quiet (bottom) halos.

3.1 Mass evolution

Figure 3a shows the total, metal-enriched stellar, and gas mass history of the most massive progenitors of both halos. The quiet halo undergoes a series of major mergers at $z > 12$, growing by a factor of 30 to $2.5 \times 10^7 M_\odot$ within 150 Myr. Afterwards it only grows by a factor of 3 by $z = 7$ mainly through smooth accretion from the filaments and IGM. It is the most massive halo in the simulation between redshifts 13 and 10. At the same time, the intense halo has a mass $M = 3 \times 10^6 M_\odot$, but it is contained in a biased region on a comoving scale of 50 kpc with ~ 25 halos with $M \sim 10^6 M_\odot$. After $z = 10$, these halos hierarchically merge to form a $10^9 M_\odot$ halo at $z = 7$ with two major mergers at redshifts 10 and 7.9, seen in the rapid increases in total mass in Figure 3a. The merger history of the two halos are not atypical as dark matter halos can experience both quiescent and vigorous mass accretion rates.

Both halos start forming Pop II stars when $M = 10^7 M_\odot$. This is consistent with the filtering mass M_f of high-redshift halos when it accretes mainly from a pre-heated IGM (Gnedin & Hui, 1998; Gnedin, 2000; Wise & Abel, 2008). Afterwards these halos can cool efficiently through H_2 cooling, sustaining constant and sometimes bursting SF. The latter characteristics are equated with the definition of a galaxy. The quiet halo forms $10^5 M_\odot$ of stars by $z = 9$. This initial starburst photo-evaporates the majority of its molecular clouds, in addition to heating and ionizing the surrounding IGM out to a radius of 10–15 kpc at $z = 9$. These respectively reduce the in-situ and external cold gas supply that could feed future SF.

The gas fractions of both halos decrease from 0.15 to 0.08 by outflows driven by ionization fronts and blastwaves in their initial starbursts. The quiet halo does not have a major merger with any halo with $M > M_f$, leading to a small final gas fraction. These low-mass halos are photo-evaporated, hosting diffuse warm gas reservoirs instead of cold dense cores. After $z = 10$, the halo mainly accretes warm diffuse gas from the filaments and IGM. In contrast, the intense halo grows from major mergers of halos with $M > M_f$. The progenitor halos involved in the major mergers are able to host molecular clouds and have higher gas fractions. Between $z = 10$ and $z = 8$, the gas
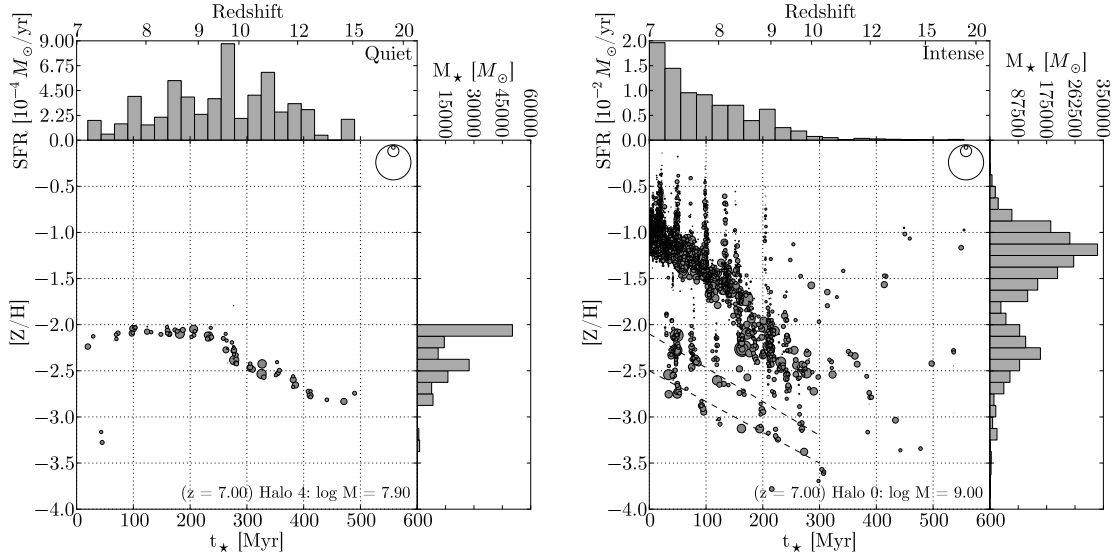
Figure 4: The scatter plots show the SF history of the quiet (left) and intense (right) halos as a function of metallicity at $z = 7$. Each circle represents a star cluster, whose area is proportional to its mass. The open circles in the upper right represent 10^3, 10^4, and 10^5 $M_\odot$ star clusters. The dashed lines in the right panel guide the eye to two stellar populations that were formed in two satellite halos, merging at $z = 7.5$. The upper histogram shows the SFR. The right histogram depicts the stellar metallicity distribution.

fraction increases from 0.07 to 0.12 until it jumps to 0.14 when a gas-rich major merger occurs. The stellar mass accordingly increases with the ample supply of gas during this period.

3.2 Metallicity evolution

The evolution of the stellar and gas metallicity of both halos are illustrated in Figure 3b. PISNe from Pop III stars enrich the nearby IGM out to a radius of 10 kpc and provides a metallicity floor of $[Z_3/H] \sim -3$. Ejecta from Pop II SNe initially enrich the ISM of both halos to an average $[\bar{Z}_2/H]$ between –3.5 and –3.

In the quiet halo, an equilibrium of $[\bar{Z}_2/H] \sim -2.5$ is established between metal-rich outflows and metal-poor inflows. Galactic outflows are directed in the polar directions of the gas disk, keeping the adjacent filaments metal-poor. These features and a well-mixed ISM (cf. Wise & Abel, 2008; Greif et al., 2010) are apparent in the metallicity projections in Figure 2. The average stellar metallicity is within 0.5 dex of $[\bar{Z}_2/H]$.

In the intense halo, the first few Pop II star clusters have $[Z/H]$ between –1 and –2 and dominate the average stellar metallicity at $z > 8$. Afterwards the metallicity increases by a factor of 30 to $[\bar{Z}_2/H] = -1.5$ through self-enrichment from a starburst. Because this halo is located in a large-scale overdensity, most of the ejecta falls back into the halo after reaching distances up to 20 comoving kpc, keeping the halo gas metallicity high because the inflows are relatively metal-rich themselves. After the $z \sim 8$ starburst, the average stellar metallicity follows the average gas metallicity within 0.1 dex.

3.3 Star formation history

The most massive progenitor of the quiet halo interestingly never hosts a Pop III star. Instead a nearby halo forms a Pop III star, which (randomly) produces a PISNe at $z = 16$. The blastwave overruns the most massive progenitor, and the dense core survives this event and is enriched by this PISN, triggering the transition to Pop II SF. Other progenitors host three Pop III stars, forming at $z = 15.4, 14.2, 13.8$, with the latter producing a PISN. Metal enrichment from these two PISNe and Pop II SF quench Pop III SF in this halo. The progenitors of the intense halo host a total of 56 Pop III stars with 21 producing PISNe. The first forms in a $6 \times 10^5 M_\odot$ halo at $z = 19$. Pop III stars form on a regular interval in the halo's progenitors until $z = 9$ when most of these halos enter the metal-rich bubble surrounding the intense halo.

Figure 4 shows the SF history (SFH), metallicity distribution, and SF rates of both halos. A nearby PISNe provides a metallicity floor of [Z/H] = –2.8 in the quiet halo at which metallicity the first Pop II stars form. The stellar metallicity evolution exhibits what is expected from an isolated system with the stellar feedback steadily enriching the ISM, resulting in a correlation between stellar age and metallicity. After $z = 10$ the metallicities plateau at [Z/H] = –2.1 for reasons previously discussed. The SFR peaks at $z = 10$ and decreases as the cold gas reservoir is depleted. Around $z = 7.5$, a 25:1 minor merger occurs, and the gas inside the satellite halo is compressed, triggering metal-poor, [Z/H] = –3.2, SF during its nearest approach. This halo remains metal-poor because most of metal enrichment in the quiet halo occurs in bi-polar flows perpendicular to the galaxy disk and filament. Stars with [Z/H] < –3 compose 1.6 percent of the total stellar mass.

In contrast with the quiet halo, the intense halo undergoes a few mergers of halos with an established stellar population. This creates a superposition of age-metallicity tracks in the SFH, seen in the complexity of Figure 4. The first two Pop II stellar clusters have an unexpectedly high metallicity [Z/H] ~ –1, which occurs when a PISN blastwave triggers SF in two neighboring halos. Most of the early SF have [Z/H] = –2.5. At $z = 9$, the halo's virial temperature reaches 10^4 K. This combined with a 10:1 merger creates a starburst that quickly enriches the halo to [Z/H] = –1.5 by $z = 8$. The halo continues to enrich itself afterwards. The spikes in the scatter plot correspond to SN triggered SF in nearby molecular clouds that are enriched up to a factor of 10 with respect to the ISM. However their mass fraction are small compared to the total stellar mass. The starburst at $z = 9$ creates a bimodal metallicity distribution with peaks at [Z/H] = –2.4 and –1.2 with the metal-rich component mainly being created after the starburst. Two systems with sizable stellar components merge into the halo at $z \sim 8$, and their stellar populations are still discernible in the metallicity-age plot. Stars with [Z/H] < –3 compose 1.8 percent of the total stellar mass.

4. Discussion and Conclusions

We focus on the birth of two galaxies prior to reionization with a cosmological AMR radiation hydrodynamics simulation. Supernovae from Pop III stars provide the necessary heavy elements for the transition to a Population II stellar population, which we have directly simulated. These two galaxies have a 10–15% probability in surviving as present-day "fossil" galaxies (Gnedin & Kravtsov, 2006), otherwise they will be incorporated into galactic stellar halos. A $z = 8.55$ galaxy was recently spectroscopically confirmed that is contained in an ionized bubble with radius 0.1– 0.5 Mpc with an uncharacterized population of galaxies contributing to the local ionizing radiation

field (Lehnert et al., 2010). The galaxies simulated here might represent this population and should be detected with the upcoming *James Webb Space Telescope*.

We find that one PISN is sufficient to enrich the star-forming halo and surrounding ~ 5 kpc to a metallicity of $10^{-3}Z_\odot$, given $M_{\mathrm{char}} = 100\ M_\odot$. DLA systems have a metallicity floor on the same order (Wolfe et al., 2005), and metal enrichment from Pop III SNe provides a possible explanation.

If the first stars have a lower characteristic mass that favor hypernovae (Tumlinson, 2007), then this metallicity floor should be lowered by a factor of ~ 10 because (1) the metal ejecta is lowered by a factor of ~ 50 and (2) the mixing mass is approximately decreased by a factor of $(E_{\mathrm{hyp}}/E_{\mathrm{PISN}})^{3/5}$ in the Sedov-Taylor solution, where $(E_{\mathrm{hyp}}/E_{\mathrm{PISN}}) \sim 0.1$ is the ratio of explosion energies of a hypernova and PISN. In the case where this metallicity floor is less than the critical metallicity, then the next instance of SF will further enrich the ISM, solidifying the transition to Pop II SF. We conclude that it only takes one, at most two, SNe from Pop III stars in the halo progenitors to complete the transition to Population II (Frebel & Bromm, 2010). The question of whether the critical metallicity is 10^{-6} or $10^{-3.5}\ Z_\odot$ is most applicable to nearby halos where the heavy elements mix slowly into dense cores as the blastwave overtakes it. Less than two percent of stars have [Z/H] < -3 in both systems, consistent with observations of metal-poor stars in the halo and dSphs (Beers & Christlieb, 2005; Battaglia et al., 2010).

We have shown that it is possible to simulate the formation of a high-redshift dwarf galaxy and its entire SFH with radiative and mechanical feedback. These results provide invaluable insight on the first galaxies and the role of metal-free stars in the early universe. There exists a wealth of information in this simulation, and we plan to follow up this preliminary report with more detailed analysis of the metal enrichment of the IGM, global SF rates, and observational connections with high-redshift galaxies and Local Group dwarf galaxies in the near future.

Acknowledgments

References

Abel, T., Anninos, P., Zhang, Y., & Norman, M. L. 1997, New Astronomy, 2, 181

Abel, T., Bryan, G. L., & Norman, M. L. 2002, Science, 295, 93

Abel, T., & Wandelt, B. D. 2002, MNRAS, 330, L53

Abel, T., Wise, J. H., & Bryan, G. L. 2007, ApJL, 659, L87

Battaglia, G., Tolstoy, E., Helmi, A., Irwin, M., Parisi, P., Hill, V., & Jablonka, P. 2010, ArXiv e-prints

Beers, T. C., & Christlieb, N. 2005, ARA&A, 43, 531

Bertschinger, E. 2001, ApJS, 137, 1

Bromm, V., Coppi, P. S., & Larson, R. B. 2002, ApJ, 564, 23

Bromm, V., Ferrara, A., Coppi, P. S., & Larson, R. B. 2001, MNRAS, 328, 969

Cen, R., & Ostriker, J. P. 1992, ApJL, 399, L113

Cen, R., & Riquelme, M. A. 2008, ApJ, 674, 644

Chabrier, G. 2003, PASP, 115, 763

Clark, P. C., Glover, S. C. O., Bonnell, I. A., & Klessen, R. S. 2009, ArXiv e-prints

Clark, P. C., Glover, S. C. O., & Klessen, R. S. 2008, ApJ, 672, 757

Ferrara, A. 1998, ApJL, 499, L17+

Frebel, A., & Bromm, V. 2010, ArXiv e-prints

Frebel, A., Kirby, E. N., & Simon, J. D. 2010, Nature, 464, 72

Gnedin, N. Y. 2000, ApJ, 542, 535

Gnedin, N. Y., & Hui, L. 1998, MNRAS, 296, 44

Gnedin, N. Y., & Kravtsov, A. V. 2006, ApJ, 645, 1054

Greif, T. H., Glover, S. C. O., Bromm, V., & Klessen, R. S. 2010, ApJ, 716, 510

Heger, A., Fryer, C. L., Woosley, S. E., Langer, N., & Hartmann, D. H. 2003, ApJ, 591, 288

Heger, A., & Woosley, S. E. 2002a, ApJ, 567, 532

—. 2002b, ApJ, 567, 532

Kitayama, T., Yoshida, N., Susa, H., & Umemura, M. 2004, ApJ, 613, 631

Komatsu, E., Smith, K. M., Dunkley, J., Bennett, C. L., Gold, B., Hinshaw, G., Jarosik, N., Larson, D., Nolta, M. R., Page, L., Spergel, D. N., Halpern, M., Hill, R. S., Kogut, A., Limon, M., Meyer, S. S., Odegard, N., Tucker, G. S., Weiland, J. L., Wollack, E., & Wright, E. L. 2010, ArXiv e-prints

Larson, R. B. 1998, MNRAS, 301, 569

Lehnert, M. D., Nesvadba, N. P. H., Cuby, J., Swinbank, A. M., Morris, S., Clément, B., Evans, C. J., Bremer, M. N., & Basa, S. 2010, Nature, 467, 940

Matsumoto, M., & Nishimura, T. 1998, ACM Trans. Model. Comput. Simul., 8, 3

Omukai, K., Tsuribe, T., Schneider, R., & Ferrara, A. 2005, ApJ, 626, 627

O'Shea, B. W., Bryan, G., Bordner, J., Norman, M. L., Abel, T., Harkness, R., & Kritsuk, A. 2004, ArXiv Astrophysics e-prints

O'Shea, B. W., & Norman, M. L. 2007, ApJ, 654, 66

Schaerer, D. 2002, A&A, 382, 28

—. 2003, A&A, 397, 527

Schneider, R., Omukai, K., Inoue, A. K., & Ferrara, A. 2006, MNRAS, 369, 1437

Smith, B., Sigurdsson, S., & Abel, T. 2008, MNRAS, 385, 1443

Smith, B. D., Turk, M. J., Sigurdsson, S., O'Shea, B. W., & Norman, M. L. 2009, ApJ, 691, 441

Stacy, A., Greif, T. H., & Bromm, V. 2010, MNRAS, 403, 45

Tafelmeyer, M., Jablonka, P., Hill, V., Shetrone, M., Tolstoy, E., Irwin, M. J., Battaglia, G., Helmi, A., Starkenburg, E., Venn, K. A., Abel, T., Francois, P., Kaufer, A., North, P., Primas, F., & Szeifert, T. 2010, ArXiv e-prints

Toro, E. F., Spruce, M., & Speares, W. 1994, Shock Waves, 4, 25, 10.1007/BF01414629

Truelove, J. K., Klein, R. I., McKee, C. F., Holliman, II, J. H., Howell, L. H., & Greenough, J. A. 1997, ApJL, 489, L179+

Tumlinson, J. 2007, ApJL, 664, L63

Turk, M. J., Abel, T., & O'Shea, B. 2009, Science, 325, 601

Turk, M. J., Smith, B. D. S., Oishi, J. S., Skory, S., Skillman, S. W., Abel, T., & Norman, M. L. 2010, ApJS, submitted (October, 2010)

Warren, M. S., Abazajian, K., Holz, D. E., & Teodoro, L. 2006, ApJ, 646, 881

Whalen, D., Abel, T., & Norman, M. L. 2004, ApJ, 610, 14

Wise, J. H., & Abel, T. 2008, ApJ, 685, 40

—. 2010, ApJS, In preparation

Wise, J. H., & Cen, R. 2009, ApJ, 693, 984

Wolfe, A. M., Gawiser, E., & Prochaska, J. X. 2005, ARA&A, 43, 861